第 44 卷 第 3 期 焊 接 学 报 Vol. 44(3):87 − 91
2023 年 3 月 TRANSACTIONS OF THE CHINA WELDING INSTITUTION March 2023

Ti 和 Nb 对铁基堆焊合金组织性能的影响

贾华[1], 高明[1], 刘政军[2]
(1. 大连海洋大学, 大连, 116023; 2. 沈阳工业大学, 沈阳, 110870)

摘要: 改变 Ti 或 Nb 的添加量制备 Fe-Cr-C-B 系铁基堆焊合金. 借助扫描电镜、X 射线衍射仪、洛氏硬度计和磨损试验机对堆焊合金组织性能进行测试分析. 结果表明, 在含 Ti 或 Nb 的堆焊合金中, 初生奥氏体晶粒细化, 共晶组织呈断网状均匀分布, 并分别有黑色圆形或块状 TiC 和菱形或三角形 NbC 硬质相颗粒生成, 添加 5%Ti 的堆焊合金组织最细小. TiC 或 NbC 硬质相颗粒在组织中呈均匀弥散分布, 能够作为耐磨质点与细化的初生奥氏体和共晶组织构成耐磨骨架, 共同抵抗磨粒的楔入与切削作用. 当 Ti 添加量为 5% 时, 含 Ti 堆焊合金达到最优耐磨性, 硬度为 66 HRC, 磨损量为 0.0487 g; 当 Nb 添加量为 4% 时, 含 Nb 堆焊合金达到最优耐磨性, 硬度为 65 HRC, 磨损量为 0.0524 g. 在同等条件下, 含有适量 Ti 的铁基堆焊合金具有更优的耐磨性.

创新点: (1) 采用自保护药芯焊丝明弧堆焊制备含 Ti 或 Nb 的 Fe-Cr-C-B 系铁基堆焊合金.
(2) 分析 Ti 或 Nb 对 Fe-Cr-C-B 系铁基堆焊合金组织性能的影响规律.
(3) 对比 TiC 和 NbC 硬质相颗粒强化效果, 使 Fe-Cr-C-B 系铁基堆焊合金获得最佳耐磨性.

关键词: 铁基堆焊合金; 自保护药芯焊丝; 明弧堆焊; 组织性能; TiC 和 NbC 颗粒
中图分类号: TG 455 **文献标识码:** A **doi:** 10.12073/j.hjxb.20220412001

0 序言

冶金、电力、农机、采矿和建材等部门每年因磨损而产生的经济损失十分巨大[1-2]. 为提高金属零件的使用寿命, 降低企业生产成本, 可采用堆焊方法对易磨损零件进行制造或再修复[3-4]. 当堆焊材料选用合金元素自保护药芯焊丝时, 整个焊接过程无需外加其它辅助保护装置, 所以更适合在恶劣工作条件下进行连续施焊[5]. 在 Fe-Cr-C-B 系堆焊合金中添加 Ti, Nb, W 和 V 等元素后, 能够生成相应的碳化物 TiC, NbC, WC 和 VC 等, 改善堆焊合金的组织性能[6-8]. 目前, 在 Ti, Nb 或 Ti 与 Nb 元素联合强化堆焊合金耐磨性方面开展的研究较多. 研究结果表明, 在液态金属凝固过程中, Ti 和 Nb 能优先与碳生成 TiC 或 NbC 硬质相颗粒, 而成为异质形核核心, 具有很强的细晶强化和弥散强化作用, 并且它们的硬度高, 与铁基体润湿性好, 对提高堆焊合金的耐磨性十分有利[7-9]. 但关于它们在同等条件下提高合金性能效果强弱方面还鲜有研究. 因此, 文中在相同外在条件和成分条件下, 采用含 Ti 或 Nb 的自保护药芯焊丝进行明弧堆焊, 制备含有不同 Ti 或 Nb 的 Fe-Cr-C-B 系铁基堆焊合金, 分析堆焊合金的显微组织与耐磨性, 确定在相同条件下 Ti 和 Nb 对堆焊合金组织性能的影响效果, 为选择适当的合金强化元素提供借鉴.

1 试验方法

堆焊药芯焊丝由钢带和药粉组成. 钢带宽度 10 mm, 厚度为 0.3 mm, 长度不受限制, 牌号为 H08A. 药粉由高碳铬铁 (质量分数, 下同)(60.6%Cr, 8.24%C)、硼铁 (18%B)、石墨 (纯度为 99.5%)、钛铁 (30%Ti) 和铁粉 (纯度>99%) 等粉末组成. 设计药芯焊丝配方时, 固定药粉中石墨、铬、硼和造渣剂 (CaF_2 + CaO + Al_2O_3 + Al 粉末) 的质量分数不变 (分别为 10%, 35%, 2% 和 4%), 改变 Ti 或 Nb 的添加量 (质量分数, 下同), 不足 100% 部分由还原铁粉补充. 因受焊丝药芯配方成分总量的限制 (为 100%), 经计算药芯中添加 Ti 元素量最多为 5%, 所

收稿日期: 2022 − 04 − 12
基金项目: 辽宁省博士科研启动基金项目 (2021-BS-237); 辽宁省教育厅高等学校基本科研项目 (LJKMZ20221108).

以改变 Ti 的添加量分别为 1%, 2%, 3%, 4% 和 5%. 为了与含 Ti 药芯焊丝配方成分形成对照，选择 Nb 的添加量也分别为 1%, 2%, 3%, 4% 和 5%. 将所用药粉过 100 目筛，烘干去除水分，混合搅拌均匀后，采用药芯焊丝成型机制成直径为 2.8 mm 的焊丝，包粉率控制在 45% ± 1% 范围内.

以研制的自保护药芯焊丝为堆焊材料，在尺寸为 100 mm × 80 mm × 12 mm 的 Q235 钢表面，采用 MZ-1000 型埋弧焊机进行明弧堆焊制备相应的合金层. 为了使堆焊层满足后续的试验要求，需要进行多层多道焊，堆焊层厚度一般为 10 mm. 堆焊工艺参数为：电弧电压 30 ~ 35 V，焊接电流 180 ~ 190 A，焊接速度 10 mm/s，焊丝伸出长度 15 mm.

堆焊试验结束后，将试样表面打磨平整. 采用 HRC-150A 型洛氏硬度计测量硬度. 制作金相试样，经体积分数 4% 的硝酸酒精溶液腐蚀后，采用 S3400N 型扫描电镜观察显微组织. 布鲁克 D8 型 X 射线衍射仪分析物相组成，其衍射范围为 15° ~ 100°. 在堆焊层表面钻取金属粉末，用化学方法分析合金成分. 采用 MLS-23 型橡胶轮式湿砂磨损试验机进行磨损试验，试样尺寸为 56 mm × 27 mm × 11 mm，磨损参数为石英砂粒度 40 目 ~ 70 目，胶轮直径 150 mm，胶轮转速 240 r/min，胶轮表面压力 1.5 MPa，磨损时间 3 min. 磨损前用分析天平测量出试样重量 M_0，将磨损后的试样清理烘干，测出磨损后重量 M_1，计算试样被磨损的重量为 $\Delta M = M_0 - M_1$，采用扫描电子显微镜观察试样的磨损形貌.

2 试验结果与讨论

2.1 X 射线衍射分析

图 1 为堆焊层的 X 射线衍射图谱. 从图中可以看出，在添加 4%Ti 或 Nb 的堆焊合金中，都存在马氏体 (M)，残余奥氏体 (A)，$(Fe,Cr)_{23}(C,B)_6$，$(Fe,Cr)_3(C,B)$ 和 $(Fe,Cr)_7(C,B)_3$ 相. 另外，在添加 4%Ti 的堆焊合金中出现 TiC 衍射峰，在添加 4%Nb 的堆焊合金中出现 NbC 衍射峰，说明添加 4%Ti 或 4%Nb 的堆焊合金中分别有初生硬质相 TiC 和 NbC 生成. 因为铬原子半径与铁相近，硼原子半径与碳相近，使得部分铬原子置换铁原子，硼原子代替碳原子，所以图谱中形成 $(Fe,Cr)_{23}(C,B)_6$，$(Fe,Cr)_3(C,B)$ 和 $(Fe,Cr)_7(C,B)_3$ 复合碳硼化物相.

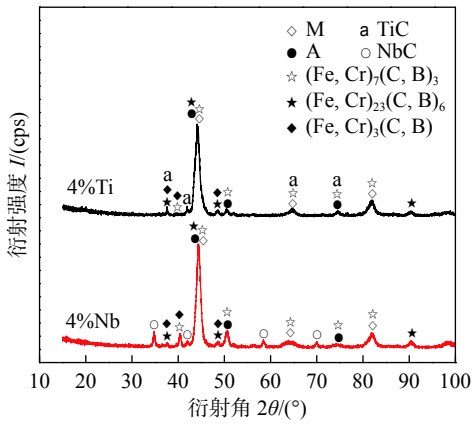

图 1 堆焊层的 X 射线衍射图谱

Fig. 1 X-ray diffraction pattern of surfacing layer

对于碳化物硬质相能否生成可以从热力学角度进行分析. 当温度和压力一定时，只有吉布斯自由能 $\Delta G_0 < 0$ 的化学反应才能发生. 在含 Ti 或 Nb 的 Fe-Cr-C-B 系铁基堆焊合金中可能发生的化学反应及各反应物的吉布斯自由能见表 1，其中 T 表示绝对温度 (K)[10].

表 1 各反应物的吉布斯自由能

Table 1 Gibbs free energy of each reactant

反应方程式	吉布斯自由能 ΔG_0/(J·mol^{-1})	温度范围 ΔT/K
$23Cr + 6C = Cr_{23}C_6$	$-309\,600 - 77.4\,T$	$298 < T < 1793$
$7Cr + 3C = Cr_7C_3$	$-153\,600 - 37.2\,T$	$298 < T < 2130$
$3Fe + C = Fe_3C$	$29\,040 - 28.03\,T$ $11\,234 - 11.0\,T$	$298 < T < 1000$ $1000 < T < 1410$
$Ti + C = TiC$	$-184\,800 + 12.55\,T$	$298 < T < 1943$
$Nb + C = NbC$	$-317\,748 + 38.851\,T$	$298 < T < 3973$

图 2 为各反应物吉布斯自由能的变化曲线. 从图中可以看出，TiC，NbC，$Cr_{23}C_6$ 和 Cr_7C_3 的吉布斯

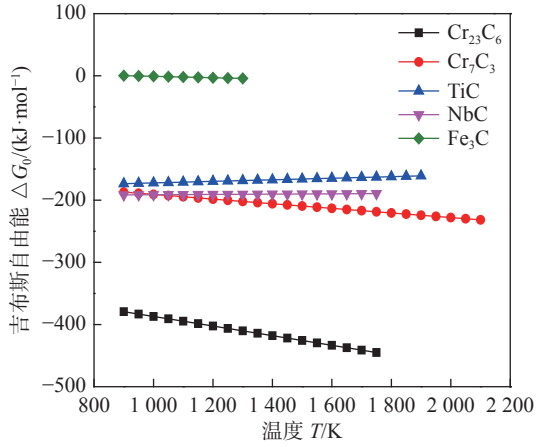

图 2 各反应物吉布斯自由能的变化曲线

Fig. 2 Variation curve of Gibbs free energy of each reactant

自由能 ΔG_0 始终小于零, 说明只要满足成分条件, 它们就能自发形成, 并在组织中稳定存在. Fe_3C 的吉布斯自由能 ΔG_0 在温度高于 1 021 K 时小于零, 说明 Fe_3C 也可以生成. 钛、铌与碳的亲和力都比铬大, 说明在满足成分条件时, TiC 和 NbC 最容易形成, 但 TiC 形成温度稍高, 所以能比 NbC 优先形成.

2.2　堆焊层硬度与耐磨性分析

为了明确 Ti 和 Nb 元素对 Fe-Cr-C-B 系铁基堆焊合金磨损性能的影响规律, 分别对堆焊层的宏观硬度和磨损量进行分析. 图 3 为不同 Ti 或 Nb 添加量时堆焊层的硬度和磨损量. 从图中可以看出, 随着 Ti 添加量的增多, 含 Ti 堆焊合金硬度明显增加, 并在 Ti 添加量为 5% 时达到最大值; 随着 Nb 添加量的增多, 含 Nb 堆焊合金硬度呈现先增加后减小的趋势, 并在 Nb 添加量为 4% 时达到最大值, 如图 3a 所示. 随着 Ti 添加量的增多, 含 Ti 堆焊合金磨损量逐渐减少, 在 Ti 添加量为 5% 时达到最小值; 而随着 Nb 添加量的增多, 含 Nb 堆焊合金磨损量呈现先减少后增加的趋势, 在 Nb 添加量为 4% 时达到最小值, 如图 3b 所示. 加入 Ti 或 Nb 后, 堆焊合金的硬度增加和磨损量减少, 应该与碳化物硬质相 TiC 或 NbC 的生成有关. 而相应曲线呈现的不同变化趋势应该与硬质相 TiC 或 NbC 的数量、形态以及分布有关.

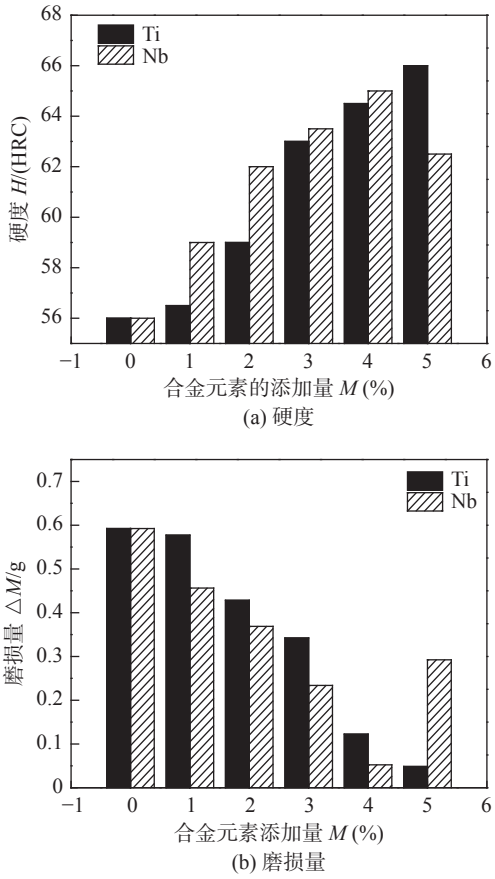

图 3　不同 Ti 或 Nb 添加量时堆焊层的硬度和磨损量

Fig. 3　Hardness and wear of surfacing layer with different addition of Ti or Nb. (a) hardness; (b) wear amount

从图 3a 和 3b 中还可以看出, 当 Ti 或 Nb 添加量在 1% ~ 4% 范围时, 含 Nb 堆焊合金硬度高, 磨损量低, 表现出较好的耐磨性; 而当 Ti 或 Nb 的添加量达到 5% 时, 含 Ti 堆焊合金硬度高, 磨损量低, 表现出较高的耐磨性. 这是由于 Ti 与 Nb 相比, Ti 的化学性质更活泼, 容易在明弧堆焊过程中与空气中的氧气反应而损失掉, 导致过渡到堆焊层中的 Ti 含量减少, 所以在 Ti 添加量较少时作用效果不明显. 但随着 Ti 添加量增多, 过渡到堆焊层中的 Ti 含量也随之增多, 促使 Ti 的作用效果显著增加. 一方面是 Ti 与 C 的亲和力大, 在满足成分条件时, TiC 能优先于 NbC 形成; 另一方面是 Ti(原子质量 48) 的原子质量比 Nb(原子质量 93) 小, 在同等合金成分条件下, Ti 能与 C 能生成更多的 TiC 硬质相. TiC(3 200 HV) 的硬度比 NbC(2 400 HV) 高, 在加上 TiC 硬质相颗粒的细晶强化和弥散强化作用, 从而使含 Ti 铁基堆焊合金表现出良好耐磨性.

在同等条件下, 通过硬度和耐磨性的对比分析可知, 当 Ti 添加量为 5% 时, 含 Ti 堆焊合金获得最优耐磨性, 硬度为 66 HRC, 磨损量为 0.048 7 g; 当 Nb 添加量为 4% 时, 含 Nb 堆焊合金达到最佳的耐磨性, 硬度为 65 HRC, 磨损量为 0.052 4 g. 因此, 在同等条件下, 含有适量 Ti 的铁基堆焊合金能够获得更优的耐磨性.

2.3　堆焊层显微组织分析

图 4 为不同试样的金相显微组织. 从图中可以看出, 未加入 Ti 或 Nb 的 Fe-Cr-C-B 系铁基堆焊合金属于典型的亚共晶组织, 主要由初生奥氏体和共晶组织 (共晶马氏体 (M) + 共晶奥氏体 (A) + $(Fe,Cr)_{23}(C,B)_6$ + $(Fe,Cr)_3(C,B)$ + $(Fe,Cr)_7(C,B)_3$ 相) 组成. 其中, 初生奥氏体晶粒粗大, 共晶组织呈连续网状分布, 组织中没有析出颗粒 (图 4a). 当添加 5%Ti 时, 初生奥氏体晶粒明显细化, 共晶组织呈断网状均匀分布, 有黑色圆形或块状 TiC 硬质相颗粒生成 (图 4b). 当添加 4%Nb 时, 初生奥氏体晶粒细化, 共晶组织也呈断网状分布, 并有菱形或三角形 NbC 硬质相颗粒生成 (图 4c). 在 Fe-Cr-C-B 系铁基堆焊合金中加入 Ti 或 Nb 元素后, 由于 Ti 或 Nb 与

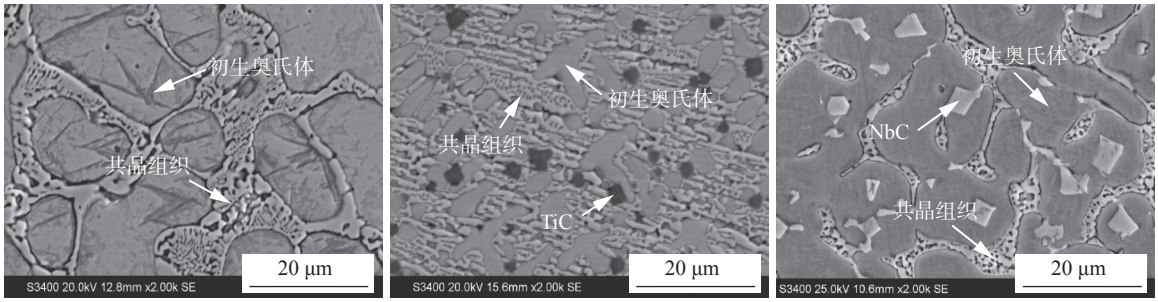

(a) 未加 Ti 或 Nb (b) 5%Ti (c) 4%Nb

图 4 不同试样的显微组织形貌

Fig. 4 Microstructure and morphology of different samples. (a) without Ti or Nb; (b) 5%Ti; (c) 4%Nb

碳的亲和力大，容易形成高熔点、高硬度的 TiC 或 NbC 初生硬质相，能够充当后续金属异质形核基底，促使形核率增加，所以加入 Ti 或 Nb 后堆焊合金的晶粒细化. 图中堆焊合金的成分见表 2.

表 2 堆焊层化学成分 (质量分数，%)

Table 2 Chemical compositions of surfacing layer

试样	Cr	C	B	Ti	Nb	Fe
未加Ti或Nb	12.96	1.48	0.52	—	—	余量
5%Ti	12.89	1.55	0.53	1.43	—	余量
4%Nb	12.82	1.57	0.52	—	1.31	余量

从图 4b 和 4c 中还可以看出，在同等条件下，含 Ti 堆焊合金中 TiC 硬质相颗粒、初生奥氏体以及共晶组织均细小，而含 Nb 堆焊合金中 NbC 硬质相颗粒和初生奥氏体晶粒相对粗大，共晶组织形态虽然没有发生变化，但数量有所减少. 这是由于 Ti 与 C 的亲和更力大，在满足成分过冷和能量起伏的条件下 TiC 容易优先形核. 优先形核的 TiC 既是初生奥氏体的形核核心，又是共晶组织的形核核心，所以含 Ti 堆焊合金组织更细小. 对于含 Nb 堆焊合金，当液态金属凝固时 NbC 将优先形核，随后长大时因 Nb 原子半径大难于扩散，只能是碳原子向 Nb 原子周围扩散堆垛，促使 NbC 晶粒长大. 含 Nb 堆焊合金碳含量一定，生成 NbC 将消耗一部分碳，将阻碍碳原子从初生奥氏体向周围液相扩散，导致共晶反应不满足成分条件而延迟发生，促使初生奥氏体晶粒长大，共晶组织减少. 优先生成的 NbC 与共晶组织互不相溶，独立存在，因此 NbC 的形成只会影响共晶组织的数量，而不会改变共晶组织的性能和尺寸[11].

2.4 堆焊层磨损形貌分析

影响试样磨损形貌的因素不仅取决于基体，也取决于碳化物的数量、分布、大小及形貌. 图 5 为不同试样的磨损形貌. 未添加 Ti 或 Nb 的试样出现大量切削沟槽，并且沟槽较深，表明其耐磨性较差，如图 5a 所示. 这是由于该堆焊层主要由初生奥氏体和共晶组织组成，没有析出硬质相颗粒，在磨粒的磨削作用下，较软的初生奥氏体基体被优先去除，而分布在周围的共晶组织又不能起到很好保护作用的缘故. 添加 5%Ti 或 4%Nb 的试样切削沟槽数量变少，深度变浅，表明其耐磨性较好，如图 5b 和 5c 所示. 这是由于加入 Ti 或 Nb 后，堆焊合金中形成均匀弥散分布的 TiC 或 NbC 硬质相，能够作为耐磨质点与细化的初生奥氏体和共晶组织构成

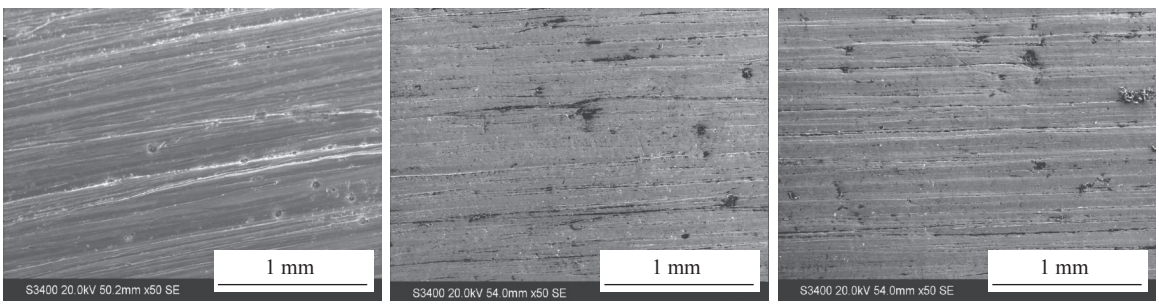

(a) 未加 Ti 或 Nb (b) 5%Ti (c) 4%Nb

图 5 不同试样的磨损形貌

Fig. 5 Wear morphology of different samples. (a) without Ti or Nb; (b) 5%Ti; (c) 4%Nb

耐磨骨架, 共同抵抗磨粒的切削作用. 另外, TiC 和 NbC 硬质相都是原位自生, 形成过程中未受污染, 界面洁净, 并且与基体组织的润湿性良好, 在磨粒作用下不易被连根拔除, 所以耐磨性较高.

对比图 5b, 图 5c 中的切削沟槽相对较多, 深度较深, 方向性明显. 一方面是组织中的 NbC 硬质相颗粒多为菱形或三角形, 存在尖角, 对基体有一定的割裂作用. 而形成的 TiC 硬质相颗粒较小, 呈块状或圆球状分布, 没有明显的尖角, 对基体的割裂作用较小. 另一方面是 TiC 尺寸细小, 晶粒比表面积大, 与基体组织之间的结合力强. 另外, 添加 5%Ti 堆焊合金的晶粒细小, 碳化物间距小, 当有磨粒磨过时, 产生在碳化物上的切削力能迅速传递到较软基体上, 能避免碳化物因应力集中产生剥落而引起二次切削. 因此, 添加 5%Ti 的铁基堆焊合金具有更为优异的耐磨性.

3　结论

(1) Ti 或 Nb 能够改变铁基堆焊合金的组织形貌. 在含 Ti 或 Nb 的堆焊合金中, 初生奥氏体晶粒细化, 共晶组织呈断网状均匀分布, 并分别有黑色圆形或块状 TiC 和菱形或三角形 NbC 硬质相颗粒生成, 当添加 5%Ti 时堆焊合金的组织最细小.

(2) Ti 或 Nb 能够提高铁基堆焊合金的硬度和耐磨性. 当 Ti 添加量为 5% 时, 含 Ti 堆焊合金达到最优耐磨性, 硬度为 66 HRC, 磨损量为 0.048 7 g; 当 Nb 添加量为 4% 时, 含 Nb 堆焊合金达到最优耐磨性, 硬度为 65 HRC, 磨损量为 0.052 4 g. 在同等条件下, 含有适量 Ti 的铁基堆焊合金具有更优的耐磨性.

(3) 在铁基堆焊层中, 高硬度的 TiC 或 NbC 颗粒呈均匀弥散分布, 能够作为耐磨质点与细化的初生奥氏体和共晶组织构成耐磨骨架, 共同抵抗磨粒的楔入与切削作用, 堆焊合金的耐磨性得以提高.

参考文献

[1] 周威, 朱协彬, 程敬卿. Fe-Cr-C-Nb 药芯焊丝堆焊合金组织与耐磨性能研究 [J]. 安徽工程大学学报, 2019, 34(3): 17 − 21.
Zhou Wei, Zhu Xiebin, Cheng Jingqing. Study on microstructure and wear resistance of Fe-Cr-C-Nb flux cored wire surfacing alloy[J]. Journal of Anhui Polytechnic University, 2019, 34(3): 17−21.

[2] 赵长春. Fe 基耐磨堆焊涂层中 (Nb, M)C 复合碳化物的结构与调控 [D]. 秦皇岛: 燕山大学, 2019.
Zhao Changchun. Structure and regulation of (Nb, M)C multiple carbide in Fe-based hardfacing coating[D]. Qinhuangdao: Yanshan University, 2019.

[3] Wang Z H, Feng M, He D Y, *et al*. The microstructure and wear resistance of Fe-Cr-C-Ti handfacing alloy[J]. Journal of Beijing University of Technology, 2013, 39(2): 275 − 279.

[4] Osetkovskiy I V, Kozyrev N A, Kryukov R E. Abrasive wear resistance comparative analysis of the metal surfaced by flux cored wires systems Fe-C-Si-Mn-Ni-Mo-W-V and Fe-C-Si-Mn-Cr-Ni-Mo-V[J]. Materials Science Forum, 2017, 906: 1 − 7.

[5] Liu H Y, Yu F B, Meng Q S, *et al*. Microstructure and properties of Fe–Cr–C hardfacing alloys reinforced with TiC-TiB_2[J]. Science and Technology of Welding and Joining, 2012, 17(5): 419 − 423.

[6] 贾华, 刘政军, 李萌, 等. 自保护药芯焊丝明弧堆焊 Fe-Cr-C-B-W 合金的组织及性能 [J]. 焊接学报, 2020, 41(3): 86 − 90.
Jia Hua, Liu Zhengjun, Li Meng, *et al*. Microstructure and properties of Fe-Cr-C-B-W alloy by self-shielded flux-cored wire open-arc surfacing[J]. Transactions of the China Welding Institution, 2020, 41(3): 86 − 90.

[7] Gou J, Liu Z J, Jia H. Effects of Nb on microstructure and wear resistance of Fe-Cr-C-B surfacing alloy[J]. Journal of Iron and Steel Research International, 2018, 25(2): 243 − 251.

[8] 刘政军, 李东芮, 王文欣, 等. TiN 对 Fe-Cr-C 耐磨堆焊合金组织及耐磨性影响 [J]. 焊接学报, 2019, 40(10): 15 − 19.
Liu Zhengjun, Li Dongrui, Wang Wenxin, *et al*. Effect of TiN on microstructure and wear resistance of Fe-Cr-C hardfacing alloy[J]. Transactions of the China Welding Institution, 2019, 40(10): 15−19.

[9] 庞雅丹, 陈伟鹏, 杨家富, 等. TiC/NbC 添加量对铁基复合材料显微组织及力学性能的影响 [J]. 稀有金属与硬质合金, 2020, 48(3): 45 − 49,86.
Pang Yadan, Chen Weipeng, Yang Jiafu, *et al*. Effect of TiC/NbC content on microstructure and mechanical properties of iron-based composite materials[J]. Rare Metals and Cemented Carbides, 2020, 48(3): 45 − 49,86.

[10] 梁英教, 车荫昌. 无机物热力学数据手册 [M]. 沈阳: 东北大学出版社, 1993.
Liang Yingjiao, Che Yinchang. Inorganic matter thermodynamics data hand book [M]. Shenyang: Northeastern University Press, 1993

[11] 田大标. 铌在高铬铸铁堆焊层中的存在状态 [J]. 中国表面工程, 2008, 21(6): 37 − 40,50.
Tian Dabiao. The status of Nb in the high Cr cast iron hardfacing layer[J]. China Surface Engineering, 2008, 21(6): 37 − 40,50.

第一作者: 贾华, 博士; 主要从事表面强化技术方面的科研和教学工作; 发表论文 10 余篇. Email: jiahua110023@126.com.

通信作者: 刘政军, 博士, 教授, 博士研究生导师; Email: liuzhengjun1962@163.com.

（编辑:　张宏强）

Abstract: In order to improve the energy utilization rate and reduce the energy dissipation, explosive welding was carried out with self-restraint structure explosive. T2 copper and Q345 steel were used as fly and base layers, respectively, and self-restraint structure explosive was adopted as welding explosive. The explosive welding process was simulated by ANSYS/AUTODYN code, and the copper/steel explosive welded clad plate was prepared. The welding quality was analyzed by mechanical property testing and microscopic morphology observation. The results show that self- restraint structure could reduce the dissipation of its own detonation products, which makes more explosive energy into kinetic energy of flyer layer and improves energy utilization rate. The collision velocity of copper/steel explosive welding is greater than the critical collision velocity of 345 m/s after detonation distance is greater than 100 mm away from the initiation end. The ultimate collision velocity at a detonation distance of 150 mm is 567 m/s. The initiation end of the copper/steel clad plate is of linear bonding, the bonding interface is transformed into wavy bonding as detonation distance increases. The shear strength of copper/steel clad plate is 237.0 MPa, and the fracture position is on the copper side. Copper layer existed work hardening after tension shear failure, and the farther measuring point from the interface is, the stronger the microhardness and plastic deformation is.

Highlights: (1) The explosive welding of copper/steel was successfully realized by using self-restraint structure explosive as welding explosive, and the microstructure and mechanical properties of composite plate were analyzed.
(2) Explosive welding process was simulated by ANSYS/AUTODYN code, and the reason that self-restraint structure explosive could reduce energy dissipation and improve utilization efficiency was analyzed.

Key words: explosive welding; self- restraint structure explosive; numerical simulation; welding quality

Effect of welding time and temperature on properties of Sn35Bi0.3Ag/Cu welded joints SHEN Bingwei, XU Mingyue, YANG Shangrong, LIU Guohua, XIE Ming, DUAN Yunzhao(Kunming Insitute of Precious Metals, State Key Laboratory of Advanced Technologies for Comprehensive Utilization of Platinum Metals, Sino-Platinum Metals Co., Ltd., Kunming 650106, China). pp 77-86

Abstract: Sn35Bi0.3Ag/Cu welded joints were prepared at different welding time and temperature. The effects of welding time (1 ~ 9 min) and welding temperature (210 ~ 290 ℃) on the microstructure and mechanical properties of Sn35Bi0.3Ag/Cu welded joints were studyed by means of scanning electron microscope (SEM), universal tensile testing machine and ultrasonic scan machine. The results show that the Cu element diffuses into the welding interface and forms the (Cu_5Sn_6, Cu_3Sn) interface layer. The Ag_3Sn phase can inhibit the growth of interfacial layer. With the increase of welding time or welding temperature, the reaction layer thickens and the shear strength increases first and then decreases. The analysis of the fracture morphology of the welded joint shows that the fracture of the welded joint is jointly affected by Bi phase particles and Cu_6Sn_5 particles. The fracture of the welded joint occurs on the IMC / solder side. Bi phase particles and Cu_6Sn_5 particles affect the shear strength of the joint. In addition, when the welding time is 3 min and the welding temperature is 230 ℃, the brazing rate is the highest (99.14%) and the shear strength reaches the maximum value (51.8 MPa).

Highlights: (1) The effects of welding time and welding temperature on the interfacial reaction and mechanical properties of Sn35Bi0.3Ag / Cu welded joints were studied.
(2) The defects of welded joints were evaluated and analyzed by ultrasonic nondestructive testing equipment.
(3) By analyzing the fracture morphology of the welded joint and combining the brazing rate and shear strengthof the joint, the optimal welding parameters are determined.

Key words: technological parameters; Sn35Bi0.3Ag/Cu welded joint; shear strength; the brazing rate

Effect of Ti and Nb on microstructure and properties of Fe based surfacing alloy JIA Hua[1], GAO Ming[1], LIU Zhengjun[2](1. Dalian Ocean University, Dalian 116023, China; 2. Shenyang University of Technology, Shenyang 110870, China). pp 87-91

Abstract: Fe-Cr-C-B Fe based surfacing alloy was prepared by changing the addition of Ti or Nb. The microstructure and properties of surfacing alloy were tested and analyzed by means of scanning electron microscope, X-ray diffraction, Rockwell hardness tester and wear tester. The results show that in the surfacing alloy containing Ti or Nb, the primary austenite grain is refined, the eutectic structure is evenly distributed in a broken network, and black circular or massive TiC and rhombic or triangular NbC hard phase particles are formed re-

spectively. The microstructure of the surfacing alloy with 5% Ti is the smallest. Tic or NbC hard phase particles are evenly dispersed in the structure and can be used as wear-resistant particles to form a wear-resistant skeleton with refined primary austenite and eutectic structure to jointly resist the wedging and cutting effect of wear particles. When the content of Ti is 5%, the surfacing alloy containing Ti achieves the best wear resistance, the hardness is 66 HRC and the wear amount is 0.048 7 g; When the addition of Nb is 4%, the surfacing alloy containing Nb achieves the best wear resistance, the hardness is 65 HRC and the wear amount is 0.052 4 g. Under the same conditions, the iron-based surfacing alloy containing an appropriate amount of Ti has better wear resistance.

Highlights: (1) The Fe-Cr-C-B iron-based surfacing alloy containing Ti or Nb is prepared by open arc surfacing with self-shielded flux-cored wire.
(2) The effect of Ti or Nb on the micro-structure and properties of Fe-Cr-C-B iron-based surfacing alloy was analyzed.
(3) Comparing the strengthening effect of TiC and NbC hard phase particles, the Fe-Cr-C-B iron-based surfacing alloy has the best wear-resistance.

Key words: iron base surfacing alloy; self-protective flux cored wire; open arc surfacing; microstructure and properties; TiC and NbC particles

Development of high power low ripple plasma spray chopper power supply WANG Dianlong[1], HUANG Hao[1], ZOU Xianxin[1], LIANG Zhimin[1], WU Chaojun[2](1. Hebei Provincial Key Laboratory of Material Near-net Forming Technology, Hebei University of Science and Technology, Shijiazhuang 050000, China; 2. Institute of Aerospace Materials and Technology, Beijing 100076, China). pp 92-97

Abstract: Plasma spraying power supply usually adopts thyristor rectifier power supply or inverter power supply, which has problems such as low efficiency and large output current ripple. It is difficult to meet the special requirements of plasma spraying process. A high-power plasma spray chopper power supply was proposed based on an eight-phase interleaved parallel Buck converter in this paper. Firstly, the circuit topology of the chopper power supply was designed. The working principle and the current ripple generation mechanism of the chopper power supply were analyzed. The influence of the number of parallel phases and the duty cycle on the current ripple was clarified. The simulation verification was carried out. Then, based on the requirements of the plasma spraying process for power supply characteristics, a four-phase interleaved parallel module with power of 40 kW was designed. Under the cooperative control of the CAN bus, an 80 kW eight-phase interleaved parallel chopper plasma spraying power supply was formed. Finally, the plasma spraying chopper power supply prototype was built. Spraying experiments were carried out to test the output ripple and efficiency of the power supply. The experimental results show that, compared with the traditional thyristor rectifier power supply and inverter power supply, the current ripple rate of the chopper power supply was reduced by more than 50%, and the power efficiency was up to 94.5%.

Highlights: (1) A plasma spray chopper power supply based on an eight-phase interleaved parallel Buck converter was proposed.
(2) Based on plasma spray chopper power supply, the controller of eight-phase interleaved parallel Buck converter was designed.

Key words: plasma spray; chopper power supply; Buck converter; interleaved parallel; current ripple

Study on temperature field, microstructure and properties of electroslag surfacing high chromium cast iron WANG Hao, HU Huie, CHI Junhan, CHEN Ze, FENG Zijian(Naval Engineering University, WuHan 430022, China). pp 98-105,113

Abstract: In this paper, the high chromium cast iron (HCCI) hardfacing layer is deposited on the surface of D32 low-alloy steel by electroslag surfacing method. Combined with the temperature field measurement of the heat-affected zone (HAZ) during the surfacing process, the microstructure and mechanical properties of the HAZ, composite interface and hardfacing layer are studied. The results show that: the heating and cooling rates are slower during the electroslag surfacing, and the temperature distribution in the low alloy steel substrate during the stabilizing stage is uniform; the maximum temperature gradient in the surfacing direction is 23.1 ℃/mm. The maximum thermal stress in the low-alloy steel substrate is 25.9 MPa, lower than its tensile strength, which effectively avoids the occurrence of cracks; the composite interface is smooth and clear, with an austenite band region, about 50 μm in width; The grains of HAZ have grown, whose microstructure is a mixture of ferrite and pearlite. The microstructure of HCCI hardfacing layer is composed of austenite, carbides and a small amount of